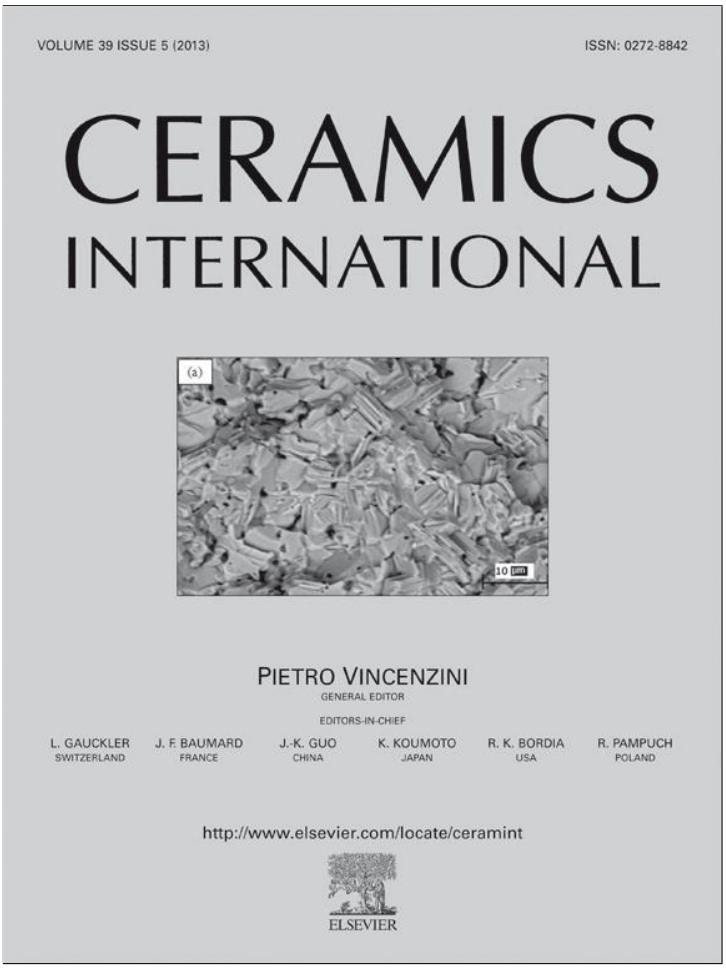

Available online at www.sciencedirect.com

SciVerse ScienceDirect

Ceramics International 39 (2013) 4777–4782

CERAMICS INTERNATIONAL

www.elsevier.com/locate/ceramint

Shielding properties of CuNiZn ferrite in the radio frequency range

María.S. Ruiz[a], Paula.G. Bercoff[b,*], Silvia.E. Jacobo[a]

[a]Laboratorio de Fisicoquímica de Materiales Cerámicos Electrónicos (LAFMACEL), Facultad de Ingeniería (UBA) – INTECIN, Paseo Colón 850, (1063) Ciudad Autónoma de Buenos Aires, Argentina

[b]Facultad de Matemática, Astronomía y Física, Universidad Nacional de Córdoba, IFEG, CONICET. M. Allende s/n, Ciudad Universitaria, 5000 Córdoba, Argentina

Received 15 August 2012; received in revised form 14 November 2012; accepted 22 November 2012
Available online 5 December 2012

Abstract

Shielding properties of copper-doped NiZn ferrites in the frequency range 1 MHz–1.8 GHz, were explored. Samples of composition $Cu_xNi_{0.4-x}Zn_{0.6}Fe_2O_4$ with $x=0.0$, 0.1, 0.2, 0.3 and 0.4, were prepared by the ceramic method. Powders and pellets were sintered at 1100 °C for 2 h. The effect of compositional variation on structural, dielectric and magnetic properties was investigated in order to relate them with the attenuation behavior. X-ray diffraction measurements confirmed the formation of a spinel structure at the selected sintering temperature. The addition of copper promotes grain growth, increases the samples density and modifies saturation magnetization, permeability and permittivity in the explored frequency range. As the reflection loss absolute values ($|R_L|$) for all the samples are above 35 dB, they can all be considered as shielding materials. The optimum attenuation was observed for $x=0.2$, reaching a maximum $|R_L|$ of almost 60 dB at 10 MHz with an attenuation bandwidth of at least 3 MHz.

Keywords: Attenuation properties; NiZn ferrites; CuZn ferrites

1. Introduction

Ferrites exhibit an interesting behavior in the radio-frequency (RF) and in the microwave (MW) range, as they absorb energy from electromagnetic waves in these ranges of frequency. For this reason, these materials have been used as absorbers in various forms, e.g., sheets, paints, films, ceramic tiles, powders and loads in matrix composites [1,2]. Among the spinel ferrites, NiZn ferrites have been widely used as electromagnetic wave absorbing materials in the VHF/UHF region [3] and as radar absorbing materials in X-band frequencies, as reported by Bueno et al. [4].

In this work, CuNiZn ferrites were synthesized by the ceramic method in order to explore the electromagnetic properties in the RF range. Ferrite of composition $Ni_{0.4}Zn_{0.6}Fe_2O_4$ was chosen as the starting system according to our previous investigations [5]. Although microwave properties of these ferrites have been studied in different frequency ranges [6,7], to our knowledge, attenuation has not been studied in frequencies between 1 MHz and 1.8 GHz.

2. Experimental

Fine ferrite powders of compositions $Cu_xNi_{0.4-x}Zn_{0.6}Fe_2O_4$, with $0 \le x \le 0.4$ were prepared by the ceramic method using metal oxides of analytical grade purity (Aldrich Sigma, Germany). Appropriate amounts of these precursors were ground and mixed thoroughly. The resulting mixture was moistened with acetone until homogenous and then it was calcined at 850 °C for 2 h. 1 wt% Bi_2O_3 (bismuth oxide) was added to the pre-sintered powders in order to increase densification and to reduce the sintering temperature [8,9]. The resulting powders were ground in a mortar, sieved and pressed with 2 ton/cm^2 in the form of pellets (1.5 cm diameter) and toroids (8 mm external diameter and 5 mm internal diameter) both with a thickness of ~1 mm. The final sintering was carried out at 1100 °C for 2 h. The spinel phase formation was confirmed by X-ray diffraction using a Rigaku diffractometer with CuKα radiation ($\lambda=1.5406$ Å). The scanning

*Corresponding author. Tel.: +54 351 4334051x103; fax: +54 351 4334054.
E-mail address: bercoff@famaf.unc.edu.ar (Paula.G. Bercoff).

0272-8842/$ - see front matter © 2012 Elsevier Ltd and Techna Group S.r.l. All rights reserved.
http://dx.doi.org/10.1016/j.ceramint.2012.11.067

range was 20–70° (2θ), with step size of 0.02 (2θ) and step time of 1 s. The data were processed for phase characterization using the software X'pert©. Experimental densities were calculated by geometry. Porosity of all samples was calculated from the JCPDS X-ray parameters for (Ni, Zn)Fe_2O_4. The microstructure was examined using a scanning electron microscope (FE-SEM Σigma Zeiss). Microanalysis was performed with an Oxford EDS system and with an electron microprobe (JEOL JXA 8230). Magnetic hysteresis loops were obtained with a vibrating sample magnetometer (LakeShore 7300) with a maximum applied field of 15 kOe. For the measurement of permittivity and permeability as a function of frequency, an impedance/material analyzer (LCR meter) in the frequency range 1 MHz–1.8 GHz (Hewlett Packard 4291 A) was used.

3. Results and discussion

3.1. Structure

X-ray diffraction patterns of the powders $Cu_xNi_{0.4-x}Zn_{0.6}Fe_2O_4$ sintered at 1100 °C for 2 h are shown in Fig. 1. The patterns display the characteristic diffraction peaks of NiZn ferrites, with a spinel structure. No secondary phases such as CuO or $CuFe_2O_4$ were detected for any of the substitutions. However, the coexistence of CuNiZn ferrite and copper oxides cannot be discarded. A secondary phase could be present in a small amount below the detection limit ($\sim < 3\%$) [10].

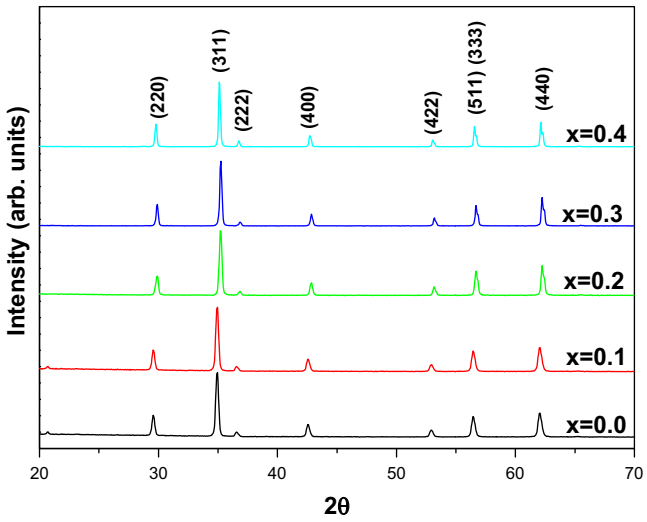

Fig. 1. X-ray diffraction patterns of $Ni_{0.4-x}Cu_xZn_{0.6}Fe_2O_4$ powders after sintering at 1100 °C for 2 h.

Cell parameters (a) are shown in Table 1 for all the studied compositions. The values of a are in the expected range for spinel ferrites [11] and slightly change with Cu substitution. As the ionic radius of Cu^{2+} (0.73 Å) is bigger than that for Ni^{2+} (0.69 Å) [12], substituting Ni^{2+} for Cu^{2+} introduces a slight increase in the cell parameter. This trend is observed up to $x=0.4$ when all Ni^{2+} has been replaced. The cell parameter for $x=0.4$ lies within the expected values for CuZn ferrite [13].

Crystallite sizes were estimated using Scherrer formula and data from XRD spectra, while grain sizes were calculated from SEM images using magnifications of 5 kx (not presented here). Both parameters increase with substitution (see Table 1). All samples show polyhedral grains, as it can be noticed in Fig. 2.

Copper substitution also increases the bulk density δ of the ferrite (see Table 1). This is related to the increase in grain size and the porosity reduction in the ferrite microstructure as shown in Fig. 2(a–e), where SEM images are displayed with the same magnetization in order to emphasize the grain size increase with Cu substitution.

The effect of Bi_2O_3 addition favors high density values [8] and prevents Zn volatilization. Porosity of all samples was estimated by comparing experimental densities with values from JCPDS X-ray parameters for (Ni, Zn)Fe_2O_4 (Table 1). EDS analysis (not shown) confirms the nominal composition for each sample.

In order to investigate the homogeneity of copper distribution in the grain boundaries as well as within the grains, electron probe microanalysis (EPMA) was performed on all samples. Cu concentration values ranging from 5 to 7 mol% were obtained in different grain boundaries (crosses marked in Fig. 3) indicating a homogenous Cu distribution within the grain boundaries. Fig. 4 shows X-ray maps of Cu, Ni and Zn. These results also support homogeneous cation distribution within the grains.

3.2. Magnetic properties

Fig. 5 shows saturation magnetization (M_S) as a function of Cu substitution. The inset shows the first quadrant of the M(H) curves for all samples. Very small coercivities (around 290 Oe) were obtained in every case.

Table 1
Cell parameter a, experimental density δ, porosity, crystallite size from Scherrer formula, grain size from SEM determinations, real permeability μ'_r and saturation magnetization M_s.

x	a (Å)	δ (g/cm^3)	Porosity (%)	Crystallite size (nm) (XRD)	Grain size (μm) (SEM)	μ'_r	M_s (emu/g)
0.0	8.391	4.3	19	33	0.4	40	57
0.1	8.396	4.8	9	40	0.9	100	65
0.2	8.408	4.8	9	35	1.9	240	73
0.3	8.413	4.7	12	44	3.9	280	63
0.4	8.406	4.9	7	51	5.2	380	39

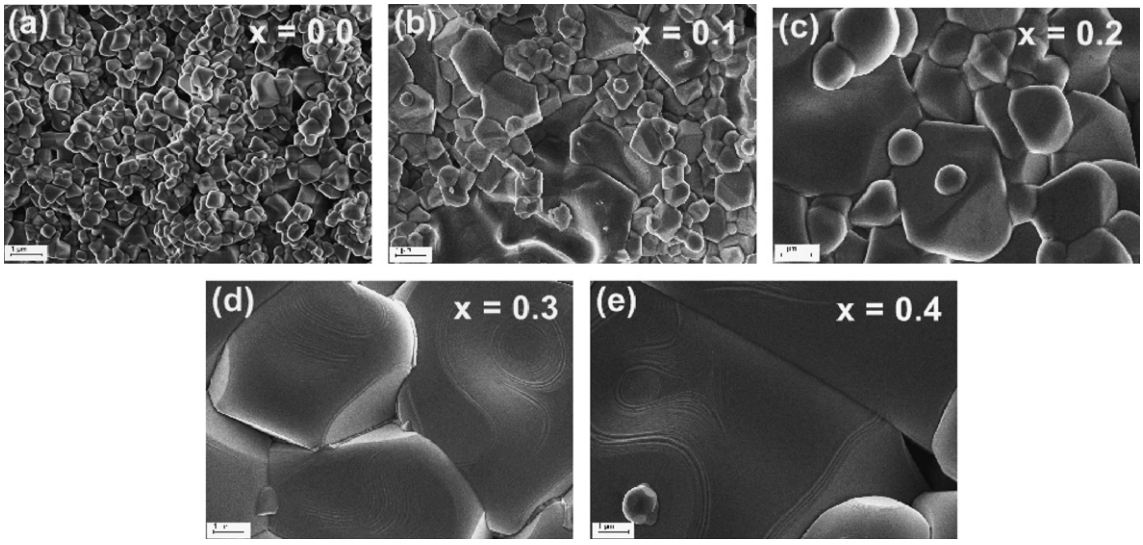

Fig. 2. (a–e) SEM images obtained with the same magnification (25 kx). The bar corresponds to 1 μm.

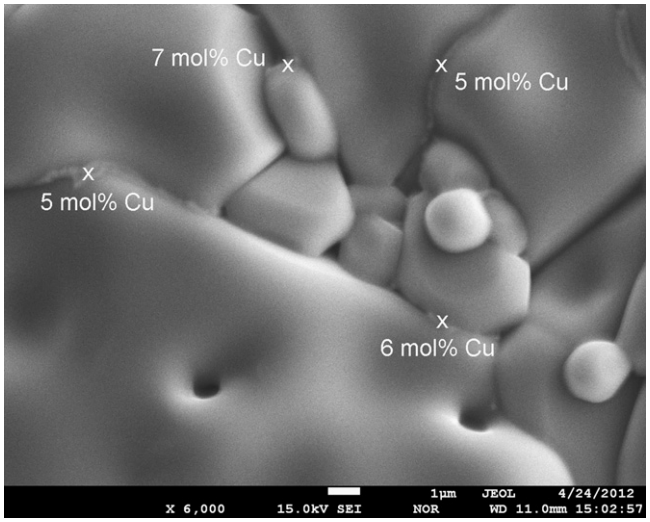

Fig. 3. SEM image of sample with $x=0.3$. The crosses marked at the grain boundaries indicate the copper concentration at those spots. The bar corresponds to 1 μm.

Magnetization in ferrites depends on factors such as chemical composition, cation distribution, crystallinity, phase segregation, porosity, grain size, etc. Particularly, it is strongly influenced by the site preference of ions in the spinel lattice. The magnetic arrangement of a spinel ferrite consists of two sub-lattices: tetrahedral (A) and octahedral (B). According to Neél's model, ferrites posses a ferrimagnetic structure in which the magnetization of the A sub-lattice is anti-parallel to that of the B sub-lattice. Within sub-lattices the individual magnetic moments are arranged parallel to one another. Following Neél's model, considering the theoretical magnetic moments ($1\mu_B$ for Cu^{2+}, $2\mu_B$ for Ni^{2+}, $0\mu_B$ for Zn^{2+} and $5\mu_B$ for Fe^{3+}) and the sites in preference of metallic ions (Zn^{2+} and Ni^{2+} have a strong preference for the A and B sites, respectively, while Fe^{3+} and Cu^{2+} may be present in both sites although they show some preference for B sites), the substitution of Ni^{2+} by Cu^{2+} ions in B sites of the spinel $Cu_xNi_{0.4-x}Zn_{0.6}Fe_2O_4$ should decrease saturation magnetization for any x. Nevertheless, M_s increases up to $x=0.2$ (Fig. 5 and/or Table 1) and decreases for further substitutions. In order to explain this discrepancy, we propose that for low Cu contents ($0 < x \leq 0.2$), some of the Cu^{2+} ions may migrate from B to A sites (i.e. limited solubility of Cu^{2+} in the B sub-lattice). Thus, a migration of Fe^{3+} ions occurs in the opposite direction, i.e. from A to B sites, changing the magnetic structure of the substituted ferrite and leading to an increase of the total magnetization with copper content. Analogous models have been corroborated by other researchers in similar systems [14,15].

For $x > 0.2$, higher Fe^{3+} migrations to the B sites may occur, introducing a decrease in the A–B superexchange interaction and consequently a decrease in the sample's saturation magnetization.

3.3. Magnetic and dielectric properties

In order to investigate attenuation properties of this system, a complete analysis of magnetic permeability and dielectric permittivity was performed.

Ni ferrites have low permeability values which are enhanced by Zn inclusion [5,16]. Fig. 6 shows the real component of the relative complex permeability ($\mu=\mu'-i\mu''$) as well as the loss factor, tan δ_μ (tan $\delta_\mu=\mu''/\mu'$) as a function of frequency for different compositions. Copper substitution increases magnetic permeability while the resonant frequency moves towards lower frequencies, as it is expected [17]. The resonant frequency is related to attenuation phenomena because when the frequency of the applied magnetic field equals the Larmor precession of the electron spins, resonance occurs and the energy is transferred from the field to the system orienting the magnetic dipoles.

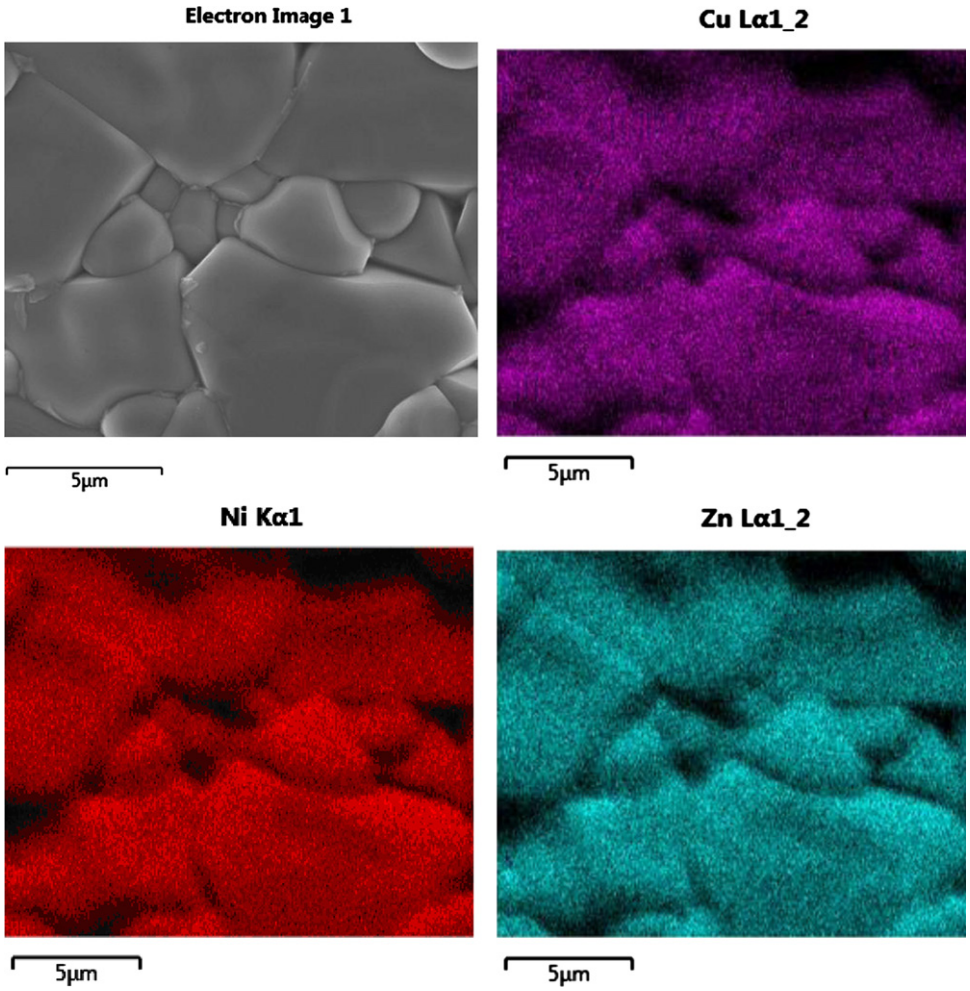

Fig. 4. FE-SEM image (top, left) and X-ray maps of Cu Ni and Zn, for sample with $x=0.3$.

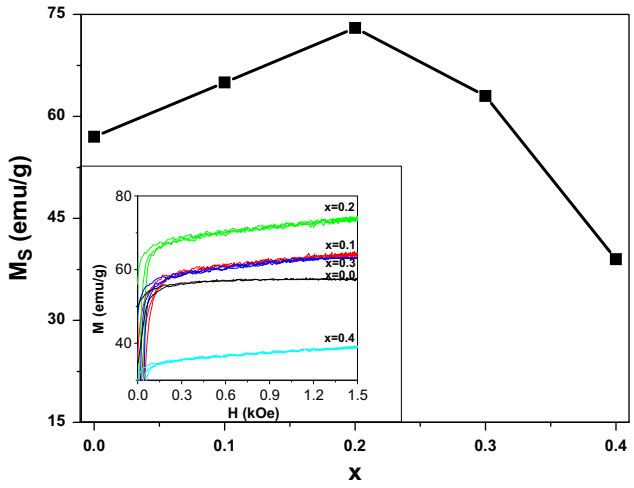

Fig. 5. Compositional variation of saturation magnetization of $Cu_xNi_{0.4-x}Zn_{0.6}Fe_2O_4$. Inset: first quadrant of M(H) curves for all samples.

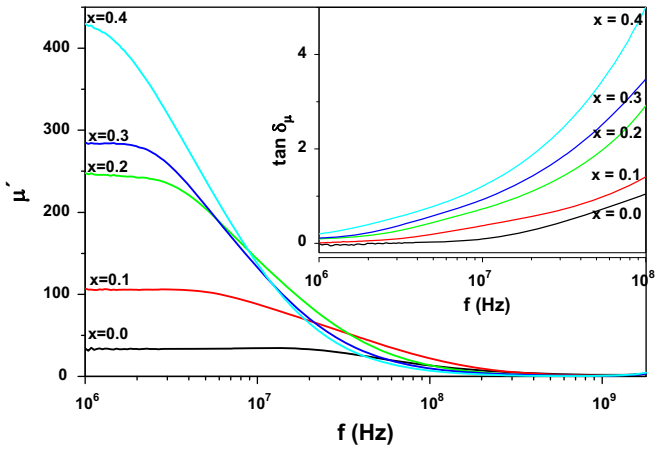

Fig. 6. Real part of magnetic permeability of $Cu_xNi_{0.4-x}Zn_{0.6}Fe_2O_4$. The inset shows the magnetic loss tangent profiles, $\tan\delta_\mu$.

As it is widely accepted, permeability in ferrites proceeds via two mechanisms, domain wall motion and domain rotation [18]. The permeability can be expressed as $\mu=1+\chi_{spin}+\chi_{dw}$, where χ_{spin} is the susceptibility due to spins and χ_{dw} is susceptibility due to domain wall motion [19]. Fig. 6 shows that the lower permeability values are observed for samples with $x=0.0$ and 0.1, probably because these samples present the smaller grain sizes (Fig. 2a and b). For the rest of the samples, higher μ' are

obtained because, among other considerations, domain wall oscillations can contribute to permeability as the grains are larger. Also, a higher μ' value is related to higher densities because there is a decrease in the intergranular porosity and hence a reduction in the demagnetizing field due to pores.

Since magnetic losses are related to the attenuation effect, tan δ_μ profiles as a function of frequency were also analyzed. For all compositions, tan δ_μ steeply increases for frequencies higher than 10 MHz (inset of Fig. 6).

Permittivity increases with Cu substitution up to $x=0.2$ and decreases for higher values (Fig. 7). The real component of the relative dielectric permittivity remains nearly constant with low values ($\varepsilon' < 8$) and the relative imaginary part ε'' is negligible for all cases ($\varepsilon'' \ll 1$, not shown in the figure). The obtained ε' values are nearly constant, possibly because the interfacial and dipolar polarizations play a dominant role at lower frequencies, decreasing their contributions with frequency.

Polarization is related to the sample density and homogeneity, among other factors. Some authors reported that Cu addition in NiZn ferrites may introduce some inhomogeneity that favors polarization, causing an increase in ε' [6]. However, in our samples the increase in ε' is mainly related to the increase in density, as we have determined a homogeneous cation distribution (Figs. 3 and 4).

The dielectric permittivity ε' is a result of the contribution of four types of polarizations, namely, interfacial, dipolar, electronic and ionic [20]. The dispersion in dielectric permittivity is more pronounced at lower frequencies than at higher frequencies.

3.3.1. Reflection loss (R_L)

Reflection loss (R_L) in ferrite absorbers can be calculated from the measured relative complex permeability ($\mu=\mu'-j\,\mu''$) and permittivity ($\varepsilon=\varepsilon'-j\,\varepsilon''$), according to [21]

$$R_L(\mathrm{dB}) = 20\log\left|Z_{in}-1\right|/\left|Z_{in}+1\right|, \quad (1)$$

being Z_{in} the relative impedance of the sample, ratio between the impedance of the sample and the impedance of the air Z_0 (377 Ω), calculated as

$$Z_{in} = \sqrt{\mu/\varepsilon}\,\tanh[-j(2\pi fD/c)(\sqrt{\mu\varepsilon})] \quad (2)$$

where c is the velocity of light (3.8×10^8 m/s), D is the sample thickness and f is the frequency (in Hz). Using the experimental values of the relative complex permeability and permittivity (Eqs. 1 and 2), it is possible to estimate the attenuation properties. Fig. 8 shows the dependence of reflection loss on frequency, for all x. For increasing copper content, the maximum $|R_L|$ is shifted to lower frequencies. A value of $|R_L|$ greater than 20 dB means that the material absorbs 99% of the input power. As the $|R_L|$ values for all the samples are above 35 dB, they can all be considered as appropriate shielding materials. The samples exhibit a relatively wide, composition-dependent attenuation bandwidth in the frequency region from 2 MHz to 40 MHz.

Fig. 9 shows the bandwidth values at $|R_L|=20$ dB for each composition. These values decrease with copper content up to $x=0.3$. The bandwidths are quite narrow, so these materials may be suitable for applications as

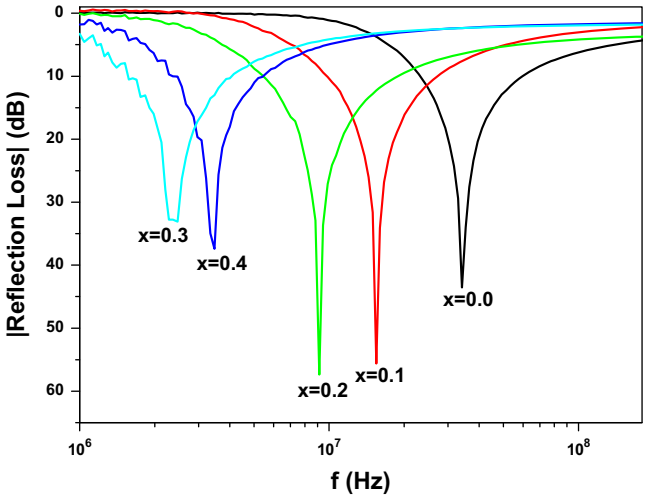

Fig. 8. Frequency dependence of reflection loss ($|R_L|$) of $Cu_xNi_{0.4-x}Zn_{0.6}Fe_2O_4$.

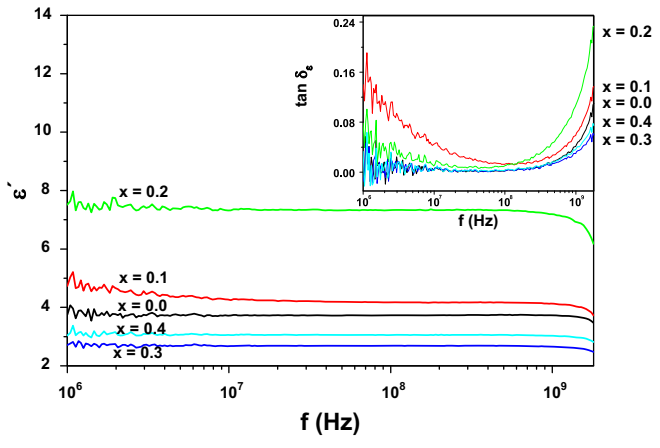

Fig. 7. Real part of dielectric permittivity ε' of $Ni_{0.4-x}Cu_xZn_{0.6}Fe_2O_4$. The inset shows the dielectric loss tangent profiles, tanδ_ε.

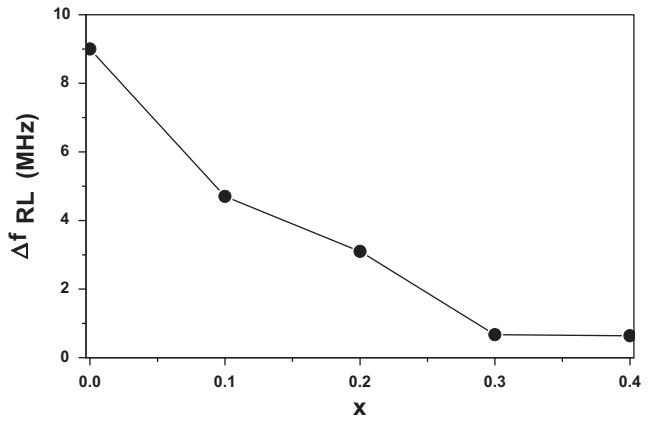

Fig. 9. Attenuation bandwidth of $Cu_xNi_{0.4-x}Zn_{0.6}Fe_2O_4$ (20 dB).

electromagnetic filters when only narrow frequency ranges are desired. Cu-substituted NiZn ferrite with $x=0.2$ reaches a maximum attenuation of $|R_L|$ ~60 dB at 10 MHz, with a bandwidth of 3 MHz.

4. Conclusions

CuNiZn ferrites were successfully prepared by the ceramic method and the influence of Cu was analyzed. XRD confirms the spinel phase for all compositions. Saturation magnetization, permeability and permittivity are modified with Cu substitution. The samples exhibit a relatively wide, composition-dependent attenuation bandwidth at frequencies from 2 MHz to 40 MHz. As the $|R_L|$ values for all the samples are above 35 dB, they can all be considered as shielding materials.

Acknowledgments

This work was partially funded by UBACyT, Secyt-UNC and CONICET. The authors are grateful to Prof. Gustavo Castellano from Lamarx for EPMA results (http://www.famaf.unc.edu.ar/lamarx).

References

[1] K. Hatakeyama, T. Inui, IEEE Transactions on Magnetics 20 (5) (1984) 1261–1263.
[2] K. Shimba, N. Tezuka, S. Sugimoto, Materials Science and Engineering B 177 (2012) 251–256.
[3] S.-S. Kim, D.-H. Han, S.-B. Cho, IEEE Transactions on Magnetics 30 (6) (1994) 4554–4556.
[4] A.R. Bueno, M.L. Gregori, M.C.S. Nóbrega, Journal of Magnetism and Magnetic Materials 320 (2008) 864–870.
[5] S.E. Jacobo, W.G. Fano, A.C. Razzitte, Physica B 320 (2002) 261–263.
[6] M.C. Dimri, A. Verma, S.C. Kashyap, D.C. Dube, O.P. Thakur, Chandra Prakash, Materials Science and Engineering B 133 (2006) 42–48.
[7] J. Shrotri, S.D. Kulkarni, C.E. Deshpande, A. Mitra, S.R. Sainkar, P.S. Anil Kumar, S.K. Date, Materials Chemistry and Physics 59 (1999) 1–5.
[8] S.F. Wang, Y.R. Wang, T.C.K. Yang, C.F. Chen, C.A. Lu, C.Y. Huang, Journal of Magnetism and Magnetic Materials 220 (2000) 129–138.
[9] A.M. El-Sayed, Ceramics International 28 (2002) 363–367.
[10] J. Mürbe, J. Töpfer, Journal of Magnetism and Magnetic Materials 324 (2012) 578–583.
[11] A.A. Sattar, H.M. El-Sayed, K.M. El-Shokrofy, M.M. El-Tabey, Journal of Applied Sciences 5 (1) (2005) 162–168.
[12] Handbook of Chemistry and Physics. 93rd edition, CRC Press, 2012–2013.
[13] E.J.W. Verwey, E.L. Heilmann, Journal of Chemical Physics 15 (1947) 174–180.
[14] U.R. Lima, M.C. Nasar, R.S. Nasar, M.C. Rezende, J.H. Araújo, J.F. Oliveira, Materials Science and Engineering B 151 (2008) 238–242.
[15] E. Rezlescu, L. Sachelarie, P.D. Popa, N. Rezlescu, IEEE Transactions on Magnetics 36 (2000) 3962–3967.
[16] J. Smit, H.P.J.Wijn, Ferrites, Eindhovan, Philips Technical Library (1959).
17] A. Globus, Journal de Physique (Paris), Colloques 1 (1977) 1.
[18] S. Chikazumi, Physics of Ferromagnetism, Claredon Press, Oxford, 1977.
[19] Nakamura, Journal of Applied Physics 88 (2000) 348–353.
[20] L.L. Hench, J.K. West, Principles of Electronic Ceramics, John Wiley, New York, 1990.
[21] E. De Fazio, P.G. Bercoff, S.E. Jacobo, Journal of Magnetism and Magnetic Materials 323 (2011) 2813–2817.